Loss of *Atg2b* and *Gskip* impairs the maintenance of the hematopoietic stem cell pool size

Shun-suke Sakai[1,#], Atsushi Hasegawa[2,#], Ryosuke Ishimura[3], Naoki Tamura[4], Shun Kageyama[3], Satoko Komatsu-Hirota[3], Manabu Abe[5], Yiwei Ling[6,7], Shujiro Okuda[6,7], Manabu Funayama[8], Mika Kikkawa[9], Yoshiki Miura[9], Kenji Sakimura[5], Ichiei Narita[1], Satoshi Waguri[4], Ritsuko Shimizu[2,*] and Masaaki Komatsu[3,*]

[1]Division of Clinical Nephrology and Rheumatology Kidney Research Center, Niigata University Graduate School of Medical and Dental Sciences, Chuo-ku, Niigata 951-8510, Japan

[2]Department of Molecular Hematology, Tohoku University School of Medicine, Sendai 980-8575, Japan

[3]Department of Physiology, [8]Research Institute for Diseases of Old Age, [9]Laboratory of Proteomics and Biomolecular Science, Biomedical Research Core Facilities, Juntendo University Graduate School of Medicine, Bunkyo-ku, Tokyo 113-8421, Japan

[4]Department of Anatomy and Histology, Fukushima Medical University School of Medicine, Hikarigaoka, Fukshima 960-1295, Japan

[5]Department of Animal Model Development, Brain Research Institute, Niigata University, Chuo-ku, Niigata 951-8585, Japan

[6]Medical AI Center, Niigata University School of Medicine, Chuo-ku, Niigata 951-8514, Japan

[7]Division of Bioinformatics, Niigata University Graduate School of Medical and Dental Sciences, Chuo-ku, Niigata 951-8514, Japan

[*]Correspondence: rshimizu@med.tohoku.ac.jp or mkomatsu@juntendo.ac.jp

[#]These authors contributed equally.

Running title: Role of ATG2B and GSKIP in HSCs

Abstract

A germline copy number duplication of chromosome 14q32, which contains *ATG2B* and *GSKIP*, was identified in families with myeloproliferative neoplasm (MPN). Herein, we show that mice lacking both *Atg2b* and *Gskip*, but not either alone, exhibited decreased hematopoiesis, resulting in death in utero accompanied by anemia. In marked contrast to MPN patients with duplication of *ATG2B* and *GSKIP*, the number of hematopoietic stem cells (HSCs), in particular long-term HSCs, in double knockout fetal livers were significantly decreased due to increased cell death. Although the remaining HSCs still had the ability to differentiate into hematopoietic progenitor cells, the differentiation efficiency was quite low. Remarkably, mice with knockout of *Atg2b* or *Gskip* alone did not show any hematopoietic abnormality. Mechanistically, while loss of both genes had no effect on autophagy, it increased the expression of genes encoding enzymes involved in oxidative phosphorylation. Taken together, our results indicate that *Atg2b* and *Gskip* play a synergistic effect in maintaining the pool size of HSCs.

Keywords: hematopoietic stem cell, hematopoiesis, *ATG2B*, *GSKIP*, autophagy, myeloproliferative neoplasm

Introduction

Myeloproliferative neoplasms (MPNs) belong to a related group of blood cancers characterized by clonal expansion of hematopoietic stem cell (HSC)-derived cells in one or more hematopoietic lineages [1, 2]. The key clinicopathological entities of MPNs are chronic myeloid leukemia, polycythemia vera, essential thrombocythemia, and primary myelofibrosis, all which are usually caused by specific somatic mutations [1, 2]. It is proposed that by disturbing various cellular mechanisms, including signaling pathways, autophagy, and cellular metabolism, MPN-initiating mutations transform HSCs into MPN stem cells that possess a survival advantage over normal HSCs [3-10]. In many cases, patients with early stage disease are clinically unremarkable and remain undiagnosed for months or years, but during this time the abnormal cells gradually replace normal blood cells and occasionally transform into malignant cells resembling genuine acute leukemic cells [1, 2].

ATG2B and *GSKIP* are located on chromosome 14q32, where a germline tandem duplication of a 700-kilobase (kb) region was identified in the pedigrees of four large West Indian families with MPNs [11]. Genetic analyses of the families revealed that germline duplication of *ATG2B* and *GSKIP* conferred a risk of familial myeloid malignancies, and overexpression of *ATG2B* and *GSKIP* in HSCs enhanced hematopoietic progenitor differentiation [11]. Both genes were also highly expressed in *de novo* acute myeloid leukemias (AMLs) [12]. Meanwhile, a genetic analysis of the pedigree of a North American family with MPNs recently showed that germline duplication of *ATG2B* and *GSKIP* genes was not required for the development of familiar myeloid malignancy syndromes associated with duplication of chromosome 14q32 [13]. The involvement of *ATG2B* and *GSKIP* in hematopoiesis and the development of MPNs and/or AMLs is thus controversial.

The protein encoding *ATG2B* is a core ATG protein that participates in autophagy [14]. Autophagy is a system in which an isolation membrane/phagophore that forms in the vicinity of the endoplasmic reticulum (ER) is elongated, and a portion of its cytoplasm is sequestered into autophagosomes, which are then transported to lysosomes for degradation [15]. The proteins involved in the formation of autophagosomes are called core ATG proteins, each of which consists of six functional units. When the ULK1 protein kinase complex1 is translocated to the ER subdomain, PI3K complex I is recruited and PI(3)P production increases. ATG18 homologues WIPI1-4 bind to PI(3)P and accumulate with their binding partners, ATG2A and 2B. ATG2A and 2B may have redundant autophagy-related functions in mammals [16], and both connect the ER to the isolation membrane/phagophore and transport lipids [16, 17]. ATG9A, a membrane protein, transiently accumulates in the isolation membrane/phagophore

and scrambles phospholipids transported by ATG2 from the ER to the cytoplasmic layer of the isolation membrane/phagophore [18 Matoba, 2020 #126]. ATG12 and ATG5 are covalently bound to each other via a ubiquitin-like conjugation reaction [19, 20]. The ATG12-ATG5 conjugate forms a complex with ATG16L and localizes to the isolation membrane/phagophore, which determines the location of amide bond formation between LC3 family proteins and PE. An LC3-PE protein called LC3-II localizes on the isolation membrane/phagophore and promotes autophagosome formation through membrane perturbation [21].

GSKIP encodes glycogen synthase kinase 3β (GSK3β) interaction protein (GSKIP). This protein is an A-kinase anchoring protein for GSK3β and PKA that regulates or facilitates their kinase activity towards their targets [22-24]. GSKIP directly interacts with GSK3β, a component of the canonical Wnt signaling pathway, and plays a critical role in embryonic development and functions as a negative regulator of GSK3β [25]. *Gskip*-deficient mouse embryos showed incomplete closure of the palatal shelves accompanied by delayed ossification along the fusion area of the secondary palatal bones, probably due to modulation of GSK3β, and caused lethality at birth [26].

Copy number variation of chromosome 14q32 upregulates the gene expression of *WIPI1*, an *ATG18* homologue, and is associated with increased conversion of LC3-I to LC3-II, suggesting that levels of autophagy are increased in patients with MPNs [11]. ATG2B is directly involved in autophagy, and GSK3β also regulates autophagy through AMPK activation and/or mTORC1 inactivation [27]. However, no studies have demonstrated a biological association between ATG2B and GSKIP. Herein, we investigated how simultaneous loss of the *Atg2b* and *Gskip* genes affected maintenance of the pool size of HSCs in mice, as well as autophagy and gene expression in *ATG2B GSKIP*-deficient human leukemia cell lines.

Results

Generation of *Atg2b Gskip* double knockout mice

As in the human genome, mouse *Atg2b* is located next to *Gskip* on chromosome 12, and both exon1 regions are adjacent (Fig. 1A). To investigate the function of Atg2b and Gskip in mice, a targeting vector was constructed by insertion of *loxP* sequences prior to and after exon1 of the *Atg2b* gene (prior to and inside exon1 of the *Gskip* gene) (Fig. 1B). Germline transmission was confirmed by Southern blot analysis (Fig. 1C). To delete the neomycin resistance gene, mice with mutant alleles were bred with *PGK-FLPo* transgenic mice (MGI ID: 4415609). The transgenic mice expressed the mouse codon-optimized FLP recombinase under the direction of the mouse phosphoglycerate kinase 1 promoter. When crossed with a strain containing a FRT

site-flanked sequence, FLPo recombinase activity was detected in all cells with complete recombinase-mediated excision of the target. The resulting progeny containing the *Atg2b Gskip*^{flox} allele were bred with *EIIa*-Cre transgenic mice (MGI ID: 2137691) to obtain *Atg2b Gskip*$^{+/-}$ heterozygous mice. *EIIa*-Cre mice carry a cre transgene under the control of the adenovirus *EIIa* promoter, which targets expression of Cre recombinase to the early mouse embryo. These mice are useful for germline deletion of loxP-flanked genes. The heterozygotes were crossbred with each other to generate *Atg2b Gskip* double knockout mice. We confirmed loss of *Atg2b* and *Gskip* transcripts as well as both proteins in *Atg2b Gskip* double-deficient mouse embryonic fibroblasts (MEFs) (Fig. 1D and E). As controls for *Atg2b Gskip*$^{-/-}$ mice, we also developed *Atg2b* and *Gskip* single knockout mice by Cas9-CRISPR technology. We targeted exon40 of *Atg2b* and exon2 of *Gskip* not to affect the expression of each gene (Fig. 2A). The generated *Atg2b*-deficient mice had 16-bp (line 1) and 4-bp (line 2) deletions of exon40, and the *Gskip*-deficient mice had a 1-bp deletion of exon2 (line1: c.33delT and line 2: c.36delC) (Fig. 2A). We used line 2 as *Atg2b* knockout mice and line 1 as *Gskip* knockout mice, and verified normal levels of the Atg2b and Gskip proteins in the *Gskip* and *Atg2b* knockout mice, respectively (Fig. 2B).

Morphological analysis of *Atg2b Gskip* double knockout mice

All *Atg2b Gskip*$^{-/-}$ mice from *Atg2b Gskip*$^{+/-}$ intercrosses died *in utero*, while *Atg2b Gskip* heterozygous (*Atg2b Gskip*$^{+/-}$) mice were born healthy and fertile with no noticeable pathological phenotype for at least 2 years. Analysis of *Atg2b Gskip*$^{-/-}$ embryos at different developmental stages showed that the majority of embryos died before embryonic day (E) 16.5 (Table 1). The *Atg2b Gskip*$^{-/-}$ embryos were not significantly smaller than their heterozygous littermates, but exhibited a severe anemic phenotype, with pale skin and subcutaneous edema along the back. Also, the mutant embryos showed exencephaly (Fig. 3A and B). Meanwhile, mice with single knockout of *Atg2b* were born at the expected Mendelian frequency (Table 1) and were viable and fertile. Like other knockout mice for *Atg* genes that have homologues [28], these knockout mice showed no noticeable pathological phenotypes for 1 year. *Gskip* knockout mice were also born at the predicted Mendelian frequency (Table 1) and were viable and fertile, which is inconsistent with the study by Deak et al. showing neonatal death [26]. This discrepancy may be due to a difference in the targeting region used. Deak's group designed the targeting vector to delete approximate 1,500 bp, including exon2 and introns 1 and 2 [26]. The targeting was accompanied by a 1,500-bp deletion about 15 kbp upstream of exon1 of *Atg2b* (Fig. 1), and may have decreased and/or abolished *Atg2b* gene expression, as with targeting

exon1 of *Gskip*. These results indicated that knocking out both *Atg2b* and *Gskip*, rather than just one of them, caused serious developmental defects in mice.

Phenotype of *Atg2b Gskip* double knockout embryos

We focused on hematological studies in the mutant mice since hematopoietic progenitor differentiation is promoted in patients with germline duplication of *ATG2B* and *GSKIP* [11]. Liver size in *Atg2b Gskip*$^{-/-}$ mice was smaller than that in control mice (Fig. 3B). Histological analysis using Meyer's hematoxylin and eosin staining showed nuclear fragmentation of cells in the livers of double knockout embryos, but not in the livers of embryos with single knockout of either *Atg2b* or *Gskip* (Fig. 3C). To examine whether loss of both *Atg2b* and *Gskip* caused cell death, we carried out immunohistochemical analysis using an antibody against cleaved Caspase-3, a hallmark of apoptosis. A marked increase in the number of cleaved Caspase-3–positive cells was noted in the livers of *Atg2b Gskip*$^{-/-}$ embryos compared with control embryos (Fig. 3D). Furthermore, the viable cells in E13.5 fetal livers were significantly decreased in *Atg2b Gskip*$^{-/-}$ embryos compared with *Atg2b Gskip*$^{+/+}$ and *Atg2b Gskip*$^{+/-}$ embryos, and consequently the absolute number of living cells in *Atg2b Gskip*$^{-/-}$ embryos was decreased (Fig. 3E). We also found that the frequency of Ter119-positive erythroid cells in the living cells was significant reduced in *Atg2b Gskip*$^{-/-}$ embryos compared with *Atg2b Gskip*$^{+/+}$ and *Atg2b Gskip*$^{+/-}$ embryos (Fig. 3F). Since erythropoiesis is a matter of the highest priority in fetal hematopoiesis and presumably in fetal development, we consider that the disturbed erythropoiesis might cause fetal liver hypoplasia and life-threatening anemia in *Atg2b Gskip*$^{-/-}$ embryos.

Concomitant reduction of *Atg2b* and *Gskip* genes causes a decrease of hematopoietic stem cells

The number of living lineage-negative (Lin(-)) cells in *Atg2b Gskip*$^{-/-}$ embryonic livers decreased compared with that in wild-type embryos (Fig. 4A). Accordingly, the number of living Lin(-)Sca1(+)ckit(+) (LSK) cells was reduced in *Atg2b Gskip*$^{-/-}$ embryos, although no significant differences in the frequency of LSK cells in Lin(-) cells were observed among the three genotype groups (Fig. 4B). On the other hand, Lin(-)CD34(-)Sca1(+)ckit(+) (CD34^{neg}-LSK) cells, which have the potential for long-term lymphohematopoietic reconstitution activity [29], were markedly reduced not only in number but also in frequency in the living Lin(-) cells in *Atg2b Gskip*$^{-/-}$ embryos compared to those in wild type (Fig. 4C). It is worth noting that the numbers of living Lin(-) cells and living LSK cells varied between *Atg2b Gskip*$^{+/-}$ embryos; some of these embryos had comparable numbers of cells as wild-type embryos, whereas the

numbers in other embryos were decreased to the level seen in *Atg2b Gskip*$^{-/-}$ embryos (Fig. 4A and B right panel). Furthermore, the absolute number and frequency of CD34^{neg}-LSK cells were decreased in *Atg2b Gskip*$^{+/-}$ embryos compared to those in wild-type embryos (Fig. 4C).

To further clarify the hematopoietic phenotype caused by concomitant reduction of *Atg2b* and *Gskip* genes, we prepared 18 embryos at E13.5 by *in vitro* fertilization of male and female *Atg2b Gskip*$^{+/-}$ mice and performed flow cytometric analysis. We divided LSK cells into five fractions, specifically long-term HSCs (LT-HSCs), short-term HSCs (ST-HSCs), and three distinct subpopulations of multi-potent progenitor cells (MPP2, MPP3, and MPP4), based on the expression profiles of CD150, CD48, and CD135 [30] (Fig. 4D). MPP2, MPP3, and MPP4 cells are defined as MPPs which are developmentally biased toward erythrocyte/megakaryocyte, monocyte/granulocyte and lymphocyte lineages, respectively [31]. As shown in Figure 4E, the frequency of LT-HSCs within LSK cells significantly decreased in *Atg2b Gskip*$^{+/-}$ embryos compared with that in wild-type embryos and further reduced in *Atg2b Gskip*$^{-/-}$ mice (Fig. 4E left panel), which was in good agreement with the result shown in Figure 4C. Thus, HSCs in heterozygous mice appeared to exhibit a haploinsufficiency phenotype. We also found that the frequency of MPP2 cells was significantly reduced in *Atg2b Gskip*$^{-/-}$ mice but was maintained in *Atg2b Gskip*$^{+/-}$ embryos. There were minimal differences in the frequencies of ST-HSCs, MPP3, and MPP4 among the three genotypes. We confirmed that there were no substantial differences in the numbers of HSC subpopulations in embryos with single knockout of either *Atg2b* or *Gskip* (Fig. 4F).

We next analyzed Lin(-)Sca1(-)ckit(+) hematopoietic precursor (LS^{neg}K) cells and found that the percentage of these cells among living Lin(-) cells was largely similar among the genotypes (Fig. 5A), suggesting that remaining HSCs in *Atg2b Gskip*$^{-/-}$ fetal livers have the ability to differentiate into hematopoietic progenitor cells. The frequencies of granulocyte-monocyte progenitor (GMP) cells, megakaryocyte-erythroid progenitor (MEP) cells, and common myeloid progenitor (CMP) cells gated on Lin(-) cells of *Atg2b Gskip*$^{-/-}$ embryos were comparable to those of *Atg2b Gskip*$^{+/-}$ and wild-type embryos, although the absolute numbers of hematopoietic precursor cells were reduced in *Atg2b Gskip*$^{-/-}$ embryos (Fig. 5B and C). Predictably, embryos of mice deficient in *Atg2b* or *Gskip* alone did not show any abnormalities in hematopoiesis (Fig. 5D). In summary, the concomitant reduction of *Atg2b* and *Gskip* genes led to a haploinsufficiency phenotype while complete loss of either the *Atg2b* or *Gskip* gene had little impact on the hematopoietic system in mice.

Hematopoietic analysis of adult mice heterozygous for the *Atg2b Gskip* knockout allele

Despite the finding that the absolute numbers of LSK, LS^{neg}K, CMP, GMP, and MEP cells varied between *Atg2b Gskip*$^{+/-}$ heterozygous mice (Figs. 4B, 5A and B), these mice were born at the expected Mendelian frequency. Furthermore, the hematopoietic indices of adult *Atg2b Gskip*$^{+/-}$ mice showed had the same values as those of *Atg2b Gskip*$^{+/+}$ mice (Fig. 6A).

We next performed flow cytometric analyses of the bone marrow of adult *Atg2b Gskip*$^{+/-}$ mice. In contrast to the findings of embryonic hematopoiesis, the frequencies of HSC/progenitor subpopulations in individual *Atg2b Gskip*$^{+/-}$ mice were virtually equivalent to those in wild-type mice (Fig. 6B-E). While fetal HSCs have the capacity to rapidly self-renew and to produce progeny in order to support hematopoiesis in developing embryos, most adult HSCs are in quiescence [32, 33]. We speculate that the differences between embryonic and adult HSCs are partly due to differences in the nature of these HSCs.

Profiling of *ATG2B*- and *GSKIP*-deficient cells

It has been reported that autophagy is critical for proper hematopoiesis [34, 35], HSC mobilization [36], and the survival of adult HSCs in the setting of acute metabolic stress [37]. Autophagy also preserves the regenerative capacity of HSCs through metabolic suppression [38]. Thus, it is plausible that loss of *ATG2B* and *GSKIP* is associated with decreased autophagy, resulting in a deficit in the blood development system. We examined whether the loss of *ATG2B, GSKIP,* or both had an effect on autophagy. To this end, we used CAS9-CRISPR technology to delete one or both genes in the human leukemia cell line K562 (Fig. 7A). The levels of LC3-II and S349-phosphorylated p62, both of which are degraded by autophagy, were comparable between both mutant K562 cell types and wild-type K562 cells (Fig. 7B). An autophagy flux assay with bafilomycin A_1 (Baf A_1), which is an inhibitor of lysosomal acidification, revealed that in both mutant K562 cell types, treatment with Baf A_1 caused up-regulation of LC3-II and S349-phosphorylated p62 to a similar extent as in parental K562 cells (Fig. 7B), indicating intact autophagy.

Finally, we conducted RNA-seq analysis with wild-type, *ATG2B*, *GSKIP*, and *ATG2B GSKIP* double knockout K562 cells. We used two pipelines, Kallisto and RSEM (RNA-Seq by Expectation Maximization), to quantify 35,619 transcripts and 26,670 genes, respectively. Multiple comparisons after ANOVA revealed that the number of genes differentially expressed in the double knockout K562 cells were 731 with Kallisto and 730 with RSEM. Hierarchical clustering exhibited gene clusters uniquely expressed in each mutant K562 cell type (Fig. 7C). Ingenuity Pathway Analysis (IPA) with transcripts and genes specified by Kallisto and RSEM identified a significant increase in oxidative phosphorylation activity in

ATG2B GSKIP double knockout K562 cells (Fig. 7D and Supplemental Table S1). Taken together, we concluded that while loss of *ATG2B* and *GSKIP* had a minimal effect on autophagy, it was accompanied by increased gene expression of enzymes involved in oxidative phosphorylation.

Excessive oxidative phosphorylation may lead to an increase in reactive oxygen species (ROS) and finally cause cell death by apoptosis [39]. We therefore evaluated the levels of apoptosis in hematopoietic stem/progenitor cells. The concurrent loss of *Atg2b* and *Gskip* increased the number of AnnexinV(+)7-Aminoactinomycin D (7-AAD)(+) late apoptotic cells in LSK, $CD34^{neg}$-LSK, CMP, GMP, and MEP fractions (Fig. 8). In addition, the numbers of AnnexinV(-)7-AAD(-) living cells in these lineages were markedly decreased in *Atg2b Gskip*$^{-/-}$ mice compared with *Atg2b Gskip*$^{+/+}$ mice, except in the GMP fraction (Fig. 8), suggesting that the apoptotic cell death of HSCs and immature progenitors might be at least in part relevant to the decreased number of hematopoietic cells in *Atg2b Gskip*$^{-/-}$ mice. In contrast to these findings, neither an increase in apoptotic cells nor a decrease in live cells was evident in these lineages in the fetal livers of *Atg2b Gskip*$^{+/-}$ mice (Fig. 8), although the number of HSCs was significantly decreased in *Atg2b Gskip*$^{+/-}$ mice (Fig. 4). We suggest that concomitant haploinsufficiency of *Atg2b* and *Gskip* may contribute to maintaining the pool size of HSCs.

Discussion

It has been suggested that regions with relatively hypoxic conditions harbor the most quiescent HSCs rather than other hematopoietic progenitors and lineage-committed precursor cells [40-42]. Glycolysis is the most important metabolic pathway in quiescent HSCs, while increases in ROS levels due to switching of the energy generation mode to mitochondrial respiration induces stem cell differentiation [43-45]. The metabolic status in HSCs is determined by many signaling pathways [43, 46]. Therefore, the regulation of metabolic conflict between glycolysis and mitochondrial respiration is a key to balancing quiescence and proliferation/differentiation in HSCs. We showed in this paper that the concomitant reduction of *Gskip* and *Atg2b* led to reduced pool size of HSCs in mice, while there were no remarkable changes in the hematopoietic system caused by single loss of either *Gskip* or *Atg2b*. Simultaneous knockout of *Gskip* and *Atg2b* increased the gene expression of enzymes involved in oxidative phosphorylation. We consider that the energy metabolism pathway of HSCs may be shifted from glycolysis to oxidative phosphorylation in mitochondria by the concomitant deficiency of Gskip or Atg2b functions, thus altering the fate of HSC.

In this regard, GSKIP is an anchoring protein for GSK3β and PKA, which are involved in the regulation of multiple cellular signaling pathways, including Wnt/β-catenin and PI3K/AKT/mTOR [22-25]. Accumulating evidence suggests that the Wnt/β-catenin and mTOR pathways play an important role in determining the fate of normal HSCs, including quiescence, self-renewal, and differentiation statuses [47, 48], and also help determine the nature of MPN stem cells [3-6]. We speculate that although mice with loss of only *Gskip* showed no particular phenotype in the hematopoietic system, probably due to functional redundancy in the signaling network in mice, deficiency of *Gskip* with concomitant ablation of *Atg2b* may be over the redundancy threshold. Since autophagy is required for erythroid differentiation [34, 35] as well as for the maintenance and mobilization of HSCs [36, 37], we considered that loss of *ATG2B* suppresses autophagic activity though not completely, thus exerting a synergistic effect with *Gskip* ablation on the pool size of HSCs. However, autophagic activity in *ATG2B* knockout and *ATG2B GSKIP* knockout K562 cells was comparable to that in parental K562 cells (Fig. 7B), probably due to redundant function of ATG2A. Actually, we verified the expression of ATG2A protein in *ATG2B* knockout and *ATG2B GSKIP* knockout K562 cells and also demonstrated similar copy numbers of both *Atg2a* and *Atg2b* transcripts in mouse embryonic LSK cells (data not shown). ATG2A is localized to isolation membranes/phagophores, but also to lipid droplets, and deficiency of both *ATG2A* and *2B* causes abnormal enlargement of these droplets [14, 49]. Since lipid droplets have the ability to scavenge ROS [50-52], cells lacking ATG2B and GSKIPmight become vulnerable to ROS.

We identified the haploinsufficiency phenotype in *Atg2b Gskip*$^{+/-}$ fetal livers although we could not observe differences in bone marrow hematopoiesis between *Atg2b Gskip*$^{+/-}$ and *Atg2b Gskip*$^{+/+}$ mice. This might be due to the differences between fetal and adult HSCs: self-renewal and proliferation are accelerated in fetal HSCs to produce abundant hematopoietic progeny in the developing embryos, while adult HSCs are largely quiescent and only occasionally enter the cell cycle to maintain hematopoietic homeostasis [32, 33]. Previous work demonstrated that oxidative metabolic pathways were activated in fetal HSCs compared with adult HSCs, and consequently total ROS levels were significantly higher in fetal livers than in BM [53]. We speculate that ROS levels in HSCs in *Atg2b Gskip*$^{+/-}$ embryos prone to go over the threshold that HSCs can change their cell-fate, leading to the phenotypic heterogeneity observed in individual *Atg2b Gskip*$^{+/-}$ embryos. In contrast, baseline ROS levels in adult HSCs are predicted to be substantially increased in *Atg2b Gskip*$^{+/-}$ HSCs, with ROS having limited influence. Although we could not identify the haploinsufficiency phenotype in A*tg2b Gskip*$^{+/-}$ adult mice at 10 weeks of age, we speculate that increased baseline ROS levels may facilitate

stem cell ageing, accompanied by the characteristic features of less frequent quiescence, myeloid bias, and DNA damage accumulation in HSCs [54].

Our experiments indicated a genetic interaction between *Atg2b* and *Gskip* and a synergistic effect of ATG2B and GSKIP on the maintenance of both HSCs and hematopoietic progenitor cells by a mechanism that is currently unknown and does not involve autophagy regulation. Our observations may provide insight into the molecular mechanisms of familial MPN and AML.

Materials and methods

Cell culture

MEFs were grown in Dulbecco's modified Eagle medium (DMEM) containing 10% fetal bovine serum (FBS), 5 U/ml penicillin, and 50 μg/ml streptomycin. K562 cells (JCRB0019) were grown in RPMI1640 medium containing 10% fetal bovine serum, 5 U/ml penicillin, and 50 μg/ml streptomycin. To generate *ATG2B* and *GSKIP* knockout K562 cells, each guide RNA designed using the CRISPR design tool (http://crispr.mit.edu/) was subcloned into pX330-U6-Chimeric_BB-CBh-hSpCas9 (42230, Addgene; deposited by Feng Zhang's lab), a human codon–optimized SpCas9 and chimeric guide RNA expression plasmid. K562 cells were co-transfected with vectors pX330 and pEGFP-C1 (6084-1; Takara Bio, Inc., Shiga, Japan), and cultured for 2 d. Thereafter, GFP-positive cells were sorted and expanded. Loss of *ATG2B* and *GSKIP* was confirmed by heteroduplex mobility assays followed by immunoblot analysis with anti-ATG2B and anti-GSKIP antibodies.

Generation of genetically modified mice

The *Atg2b Gskip*–targeting vector was constructed by insertion of *loxP* sequences prior to and after exon1 of the *Atg2b* gene (prior to and inside of exon1 of the *Gskip* gene). The targeting vectors were electroporated into mouse RENKA ES cells, selected with G418 (250 μg/ml; Invitrogen, San Diego, CA), and then screened for homologous recombinants by Southern blot analysis. Southern blot analysis in *Atg2b Gskip*^{flox} mice was performed by digesting genomic DNA with *Spe*I (Takara Bio, Inc.) or *EcoR*I (Takara Bio, Inc.), followed by hybridization to detect wild-type 16.5-kb and flox 9-kb bands or wild-type 10.5-kb and flox 8.9-kb bands.

To generate single *Atg2b*- and *Gskip*-deficient mice by CRISPR-Cas technology, CRISPR RNAs (crRNAs) were designed to recognize target sites (exon40 of *Atg2b*: 5'-AAGGATGGCCGTATCGTCAG-3' and exon2 of *Gskip*: 5'- GGAAACAGACTATAATCCCG-3'). The synthetic crRNAs (Alt-R™ CRISPR-Cas9 crRNA), tracrRNA (Alt-R™ CRISPR-Cas9

tracrRNA), and Cas9 protein (Alt-R™ S.p. Cas9 Nuclease 3NLS) were purchased from Integrated DNA Technologies, Inc. (IDT) (Coralville, IA). The CRISPR/Cas9 solution was prepared as previously described [55], with minor modifications. Briefly, lyophilized crRNAs and tracrRNA were resuspended in Nuclease-Free Duplex Buffer (IDT) to a concentration of 240 μM. Equal volumes of crRNA and tracrRNA were combined, heated at 95°C for 5 min, and then placed at room temperature (RT) for about 10 min to allow formation of crRNA:tracrRNA duplex. The crRNA:tracrRNA duplex was mixed with Cas9 protein to form a ribonucleoprotein complex in Opti-MEM (Thermo Fisher Scientific,Waltham, Massachusetts). The final concentrations of Cas9 protein and crRNA:tracrRNA duplex were 1 μg/μl and 30 μM, respectively. To induce CRISPR/Cas9-mediated deletion/insertion, we applied a recently developed method called improved Genome-editing via Oviductal Nucleic Acids Delivery [55]. Approximately 1.5 μl of CRISPR/Cas9 solution was injected into the oviductal lumens of female C57BL/6N mice at day 0.7 of pregnancy. Immediately after the injection, the oviduct regions were grasped with a tweezer-type electrode (CUY652-3; Nepa Gene Co., Ltd., Chiba, Japan) and then electroporated using the NEPA21 square-wave pulse generator (Nepa Gene). The electroporation parameters used were as previously described [55]. Pregnant female mice were allowed to deliver their pups. Tail biopsies of pups were performed for genomic DNA isolation.

RT-qPCR (real-time quantitative reverse transcription PCR)

Using the Transcriptor First-Strand cDNA Synthesis Kit (Roche Applied Science, Indianapolis, IN), cDNA was synthesized from 1 μg of total RNA. RT-qPCR was performed using the LightCycler® 480 Probes Master mix (Roche Applied Science) on a LightCycler® 480 (Roche Applied Science). Signals from mouse samples were normalized against *Gusb* (ß-glucuronidase) mRNA. The sequences of the primers used were: *Atg2b* Left, TTTTGCACCAAAAACAGTCG; *Atg2b* Right, CGTCGTCAACCATGTCTTTATC; *Gskip* Left, GGAGCAAAGGAAAGGAACAGA; and *Gskip* Right, TCAAAACATAGCCCACCA.

Immunoblot analysis

Mouse livers and brains were homogenized in 0.25 M sucrose, 10 mM 2-(4-[2-hydroxyethyl-1-piperazinyl)ethanesulfonic acid (HEPES) (pH 7.4), and 1 mM dithiothreitol (DTT). Cells were lysed with TNE buffer (20 mM Tris-Cl, pH 7.5, 0.5% Nonidet P-40, 150 mM NaCl, 1 mM ethylenediaminetetraacetic acid [EDTA], and 1 mM DTT containing protease inhibitor cocktail (Roche Applied Science). Samples were subjected to SDS-PAGE, then transferred to a

polyvinylidene difluoride membrane (IPVH00010; Merck). Antibodies against Atg2b (25155-1-AP, 1:500; Proteintech Group, Inc., IL, USA), Gskip (#PA5-60218, 1:500; Thermo Fisher Scientific), LC3B (#2775, 1:500; Cell Signaling Technology, Boston, MA, USA), and Actin (MAB1501R, 1:1000; Merck Millipore, Burlington, MA) were purchased from the indicated suppliers. Blots were incubated with horseradish peroxidase–conjugated goat anti-mouse IgG (H+L) (115-035-166; Jackson ImmunoResearch Laboratories, Inc., West Grove, PA), goat anti-rabbit IgG (H+L) (111-035-144; Jackson ImmunoResearch Laboratories, Inc.), or goat anti-guinea pig IgG (H+L) antibody (106-035-003; Jackson ImmunoResearch Laboratories, Inc.), and visualized by chemiluminescence. Band density was measured using the software Multi Gauge V3.2 (FUJIFILM Corporation, Tokyo, Japan).

Histological analysis

Excised liver tissues were fixed by immersion in 0.1 M phosphate buffer (PB, pH 7.4) containing 4% paraformaldehyde and 4% sucrose. Embryos were delivered, and their livers were fixed by immersion in 0.1 M PB (pH 7.4) containing 4% paraformaldehyde and 4% sucrose. Each liver was carefully dissected and processed for paraffin embedding, and then sections were prepared for hematoxylin and eosin staining. Images were captured with a BX51 microscope (Olympus, Tokyo, Japan). For detection of apoptotic cells, sagittal serial sections with 3-um thickness were prepared for each embryo. Three to 6 sections were selected at intervals of 90-160 um, and immunostained with anti-cleaved Caspase-3 (#9661, 1:500; Cell Signaling Technology). Images were captured with a BX53 microscope (Olympus). For quantification, the number of cleaved Caspase-3–positive cells per mm^2 in each liver section was counted.

Flow cytometry

For cell population analyses, lineage depletion was performed using a cocktail of biotinylated antibodies against Ter119, B220, Gr1, CD4, CD8, and CD127, followed by their removal using Dynabeads M-280 streptavidin–-conjugated magnetic beads (Thermo Fisher Scientific). Lin(-) hematopoietic stem and progenitor cells (HSPCs) were stained with a combination of allophycocyanin (APC)-conjugated anti-CD34, fluorescein isothiocyanate (FITC)–conjugated anti-CD48, phycoerythrin (PE)-conjugated or Brilliant Violet 510 (BV510) anti-CD150, PE-conjugated anti-CD135, APC-eFluor 780 (APC-eF780)–conjugated anti-ckit, PE-Cyanin 7 (PE-Cy7)–conjugated anti-CD16/32, and Brilliant Violet 421 (BV421)–conjugated anti-Sca1. Dead cells were excluded by 7-AAD. For apoptotic cell analysis, lineage-negative HSPCs were

stained with a combination of APC-conjugated anti-CD34, PE-Cy7–conjugated anti-CD16/32, APC-eF780–conjugated anti-ckit, BV421-conjugated anti-Sca1, FITC-conjugated anti-Annexin V, and 7-AAD. Stained cells were analyzed with a BD FACSAria II flow cytometer and BD FACSDiva software (Becton Dickinson, Franklin Lakes, NJ). Information regarding antibodies is available upon request.

Differential expression analysis

Read mapping was conducted according to the GRCh38 reference genome using STAR software (Spliced Transcripts Alignment to a Reference) v2.7.7a [56], then gene and isoform expression were quantified by RSEM v1.3.3 [57]. RNA-seq analysis was also performed by Kallisto using Ensembl Homo sapiens GRCh38 cDNA transcripts (release 104) for indexing. Transcript-level quantification was examined by Kallisto version 0.46.2 [58] using 100 bootstrap samples. Excepted counts of 12 samples in four groups on the gene level, obtained with RSEM or Kallisto, were used for differential expression analysis with DESeq2 [59]. Estimated counts of transcript level obtained with Kallisto were mapped and switched using Ensembl GRCh38 release 98. In detail, the significance of the change in deviance between the four groups was tested by the likelihood ratio test, and post-hoc tests between the three knockout groups and the wild-type group were conducted by Wald's test. All p-values generated by the above tests were adjusted by the Hochberg method [60]. Differentially expressed genes present only in double knockout mice were defined as those that were significant in double knockout vs wild type mice, and nonsignificant in both of the single knockout mice vs wild type mice, with a significance level set to 5%. TPM values of differentially expressed genes occurring only in double knockout mice were used to explore specially expressed gene clusters for each group by hierarchical clustering, with the Euclidean distance method and Ward clustering method. The clustering results are shown by heatmap. All statistical tests and preparation of graphics were performed by software R v4.0.0 (https://www.r-project.org/). Ingenuity pathway analysis (IPA, released September 2021, QIAGEN Redwood City, http://www.ingenuity.com/) was used to identify significant canonical pathways involving the differentially expressed genes enriched using the above two methods.

Author contributions

S-s.S., A.H., R.I., N.T., S.K., and S.W. performed most of the experiments characterizing the knockout mice. S.K-H. generated the genetic modified K562 cells. M.A. and K.S. generated the genetically modified mice. W.L., S.O., and M.F. analyzed the RNA-seq data. M.K. and Y.M.

carried out the Ingenuity Pathway Analysis with RNA-seq data. R.S. and M.Komatsu conceived the experiments. I.N. provided intellectual support. R.S. and M.Komatsu wrote the manuscript. All authors discussed the results and commented on the manuscript.

Acknowledgements

We thank K. Kanno (Fukushima Medical University) for his help in histological analyses. We also thank the Laboratory of Biomedical Research Resources, Biomedical Research Core Facilities, and Juntendo University Graduate School of Medicine, for technical assistance with *in vitro* fertilization. M.K. is supported by a Grant-in-Aid for Scientific Research on Innovative Areas (19H05706), a Grant-in-Aid for Scientific Research (A) (21H004771), the Japan Society for the Promotion of Science (an A3 foresight program), and the Takeda Science Foundation (to M.K.). This work was supported by JSPS KAKENHI Grant Number JP 16H06276 (AdAMS).

References

1. Shallis RM, Wang R, Davidoff A, Ma X, Podoltsev NA and Zeidan AM (2020) Epidemiology of the classical myeloproliferative neoplasms: The four corners of an expansive and complex map. Blood Rev 42:100706. doi: 10.1016/j.blre.2020.100706
2. Tefferi A (2016) Myeloproliferative neoplasms: A decade of discoveries and treatment advances. Am J Hematol 91:50-8. doi: 10.1002/ajh.24221
3. Zhou H, Mak PY, Mu H, Mak DH, Zeng Z, Cortes J, Liu Q, Andreeff M and Carter BZ (2017) Combined inhibition of beta-catenin and Bcr-Abl synergistically targets tyrosine kinase inhibitor-resistant blast crisis chronic myeloid leukemia blasts and progenitors in vitro and in vivo. Leukemia 31:2065-2074. doi: 10.1038/leu.2017.87
4. Lucijanic M, Livun A, Tomasovic-Loncaric C, Stoos-Veic T, Pejsa V, Jaksic O, Prka Z and Kusec R (2016) Canonical Wnt/beta-Catenin Signaling Pathway Is Dysregulated in Patients With Primary and Secondary Myelofibrosis. Clin Lymphoma Myeloma Leuk 16:523-526. doi: 10.1016/j.clml.2016.06.004
5. Cokic VP, Mossuz P, Han J, Socoro N, Beleslin-Cokic BB, Mitrovic O, Suboticki T, Diklic M, Lekovic D, Gotic M, Puri RK, Noguchi CT and Schechter AN (2015) Microarray and Proteomic Analyses of Myeloproliferative Neoplasms with a Highlight on the mTOR Signaling Pathway. PLoS One 10:e0135463. doi: 10.1371/journal.pone.0135463
6. Greenfield G, McMullin MF and Mills K (2021) Molecular pathogenesis of the myeloproliferative neoplasms. J Hematol Oncol 14:103. doi: 10.1186/s13045-021-01116-z
7. Helgason GV, Mukhopadhyay A, Karvela M, Salomoni P, Calabretta B and Holyoake TL (2013) Autophagy in chronic myeloid leukaemia: stem cell survival and implication in therapy. Curr Cancer Drug Targets 13:724-34. doi: 10.2174/15680096113139990088
8. Baquero P, Dawson A, Mukhopadhyay A, Kuntz EM, Mitchell R, Olivares O, Ianniciello A, Scott MT, Dunn K, Nicastri MC, Winkler JD, Michie AM, Ryan KM, Halsey C, Gottlieb E, Keaney EP, Murphy LO, Amaravadi RK, Holyoake TL and Helgason GV (2019) Targeting quiescent leukemic stem cells using second generation autophagy inhibitors. Leukemia 33:981-994. doi: 10.1038/s41375-018-0252-4
9. Zhang H, Li H, Xi HS and Li S (2012) HIF1alpha is required for survival maintenance of chronic myeloid leukemia stem cells. Blood 119:2595-607. doi: 10.1182/blood-2011-10-387381

10. Rao TN, Hansen N, Hilfiker J, Rai S, Majewska JM, Lekovic D, Gezer D, Andina N, Galli S, Cassel T, Geier F, Delezie J, Nienhold R, Hao-Shen H, Beisel C, Di Palma S, Dimeloe S, Trebicka J, Wolf D, Gassmann M, Fan TW, Lane AN, Handschin C, Dirnhofer S, Kroger N, Hess C, Radimerski T, Koschmieder S, Cokic VP and Skoda RC (2019) JAK2-mutant hematopoietic cells display metabolic alterations that can be targeted to treat myeloproliferative neoplasms. Blood 134:1832-1846. doi: 10.1182/blood.2019000162

11. Saliba J, Saint-Martin C, Di Stefano A, Lenglet G, Marty C, Keren B, Pasquier F, Valle VD, Secardin L, Leroy G, Mahfoudhi E, Grosjean S, Droin N, Diop M, Dessen P, Charrier S, Palazzo A, Merlevede J, Meniane JC, Delaunay-Darivon C, Fuseau P, Isnard F, Casadevall N, Solary E, Debili N, Bernard OA, Raslova H, Najman A, Vainchenker W, Bellanne-Chantelot C and Plo I (2015) Germline duplication of ATG2B and GSKIP predisposes to familial myeloid malignancies. Nat Genet 47:1131-40. doi: 10.1038/ng.3380

12. Pegliasco J, Schmaltz-Panneau B, Martin JE, Chraibi S, Khalife-Hachem S, Salviat F, Pasquier F, Willekens C, Lopez M, Ben-Ali A, Bera O, Caron O, Castilla-Llorent C, Cotteret S, Bourdin C, Saada V, Auger N, de Botton S, Vainchenker W, Fuseau P, Helias P, Benabdelali R, Marzac C, Meniane JC, Plo I, Bellanne-Chantelot C and Micol JB (2021) ATG2B/GSKIP in de novo acute myeloid leukemia (AML): high prevalence of germline predisposition in French West Indies. Leuk Lymphoma 62:1770-1773. doi: 10.1080/10428194.2021.1881508

13. Babushok DV, Stanley NL, Morrissette JJD, Lieberman DB, Olson TS, Chou ST and Hexner EO (2018) Germline duplication of ATG2B and GSKIP genes is not required for the familial myeloid malignancy syndrome associated with the duplication of chromosome 14q32. Leukemia 32:2720-2723. doi: 10.1038/s41375-018-0231-9

14. Velikkakath AK, Nishimura T, Oita E, Ishihara N and Mizushima N (2012) Mammalian Atg2 proteins are essential for autophagosome formation and important for regulation of size and distribution of lipid droplets. Mol Biol Cell 23:896-909. doi: 10.1091/mbc.E11-09-0785

15. Nakatogawa H (2020) Mechanisms governing autophagosome biogenesis. Nat Rev Mol Cell Biol 21:439-458. doi: 10.1038/s41580-020-0241-0

16. Valverde DP, Yu S, Boggavarapu V, Kumar N, Lees JA, Walz T, Reinisch KM and Melia TJ (2019) ATG2 transports lipids to promote autophagosome biogenesis. J Cell Biol 218:1787-1798. doi: 10.1083/jcb.201811139

17. Osawa T, Kotani T, Kawaoka T, Hirata E, Suzuki K, Nakatogawa H, Ohsumi Y and Noda NN (2019) Atg2 mediates direct lipid transfer between membranes for autophagosome formation. Nat Struct Mol Biol 26:281-288. doi: 10.1038/s41594-019-0203-4

18. Maeda S, Yamamoto H, Kinch LN, Garza CM, Takahashi S, Otomo C, Grishin NV, Forli S, Mizushima N and Otomo T (2020) Structure, lipid scrambling activity and role in autophagosome formation of ATG9A. Nat Struct Mol Biol 27:1194-1201. doi: 10.1038/s41594-020-00520-2

19. Huang D, Xu B, Liu L, Wu L, Zhu Y, Ghanbarpour A, Wang Y, Chen FJ, Lyu J, Hu Y, Kang Y, Zhou W, Wang X, Ding W, Li X, Jiang Z, Chen J, Zhang X, Zhou H, Li JZ, Guo C, Zheng W, Zhang X, Li P, Melia T, Reinisch K and Chen XW (2021) TMEM41B acts as an ER scramblase required for lipoprotein biogenesis and lipid homeostasis. Cell Metab. doi: 10.1016/j.cmet.2021.05.006

20. Ghanbarpour A, Valverde DP, Melia TJ and Reinisch KM (2021) A model for a partnership of lipid transfer proteins and scramblases in membrane expansion and organelle biogenesis. Proc Natl Acad Sci U S A 118. doi: 10.1073/pnas.2101562118

21. Maruyama T, Alam JM, Fukuda T, Kageyama S, Kirisako H, Ishii Y, Shimada I, Ohsumi Y, Komatsu M, Kanki T, Nakatogawa H and Noda NN (2021) Membrane perturbation by lipidated Atg8 underlies autophagosome biogenesis. Nat Struct Mol Biol 28:583-593. doi: 10.1038/s41594-021-00614-5

22. Dema A, Schroter MF, Perets E, Skroblin P, Moutty MC, Deak VA, Birchmeier W

and Klussmann E (2016) The A-Kinase Anchoring Protein (AKAP) Glycogen Synthase Kinase 3beta Interaction Protein (GSKIP) Regulates beta-Catenin through Its Interactions with Both Protein Kinase A (PKA) and GSK3beta. J Biol Chem 291:19618-30. doi: 10.1074/jbc.M116.738047

23. Loh JK, Lin CC, Yang MC, Chou CH, Chen WS, Hong MC, Cho CL, Hsu CM, Cheng JT, Chou AK, Chang CH, Tseng CN, Wang CH, Lieu AS, Howng SL and Hong YR (2015) GSKIP- and GSK3-mediated anchoring strengthens cAMP/PKA/Drp1 axis signaling in the regulation of mitochondrial elongation. Biochim Biophys Acta 1853:1796-807. doi: 10.1016/j.bbamcr.2015.04.013

24. Chou HY, Howng SL, Cheng TS, Hsiao YL, Lieu AS, Loh JK, Hwang SL, Lin CC, Hsu CM, Wang C, Lee CI, Lu PJ, Chou CK, Huang CY and Hong YR (2006) GSKIP is homologous to the Axin GSK3beta interaction domain and functions as a negative regulator of GSK3beta. Biochemistry 45:11379-89. doi: 10.1021/bi061147r

25. Hundsrucker C, Skroblin P, Christian F, Zenn HM, Popara V, Joshi M, Eichhorst J, Wiesner B, Herberg FW, Reif B, Rosenthal W and Klussmann E (2010) Glycogen synthase kinase 3beta interaction protein functions as an A-kinase anchoring protein. J Biol Chem 285:5507-21. doi: 10.1074/jbc.M109.047944

26. Deak VA, Skroblin P, Dittmayer C, Knobeloch KP, Bachmann S and Klussmann E (2016) The A-kinase Anchoring Protein GSKIP Regulates GSK3beta Activity and Controls Palatal Shelf Fusion in Mice. J Biol Chem 291:681-90. doi: 10.1074/jbc.M115.701177

27. Mancinelli R, Carpino G, Petrungaro S, Mammola CL, Tomaipitinca L, Filippini A, Facchiano A, Ziparo E and Giampietri C (2017) Multifaceted Roles of GSK-3 in Cancer and Autophagy-Related Diseases. Oxid Med Cell Longev 2017:4629495. doi: 10.1155/2017/4629495

28. Kuma A, Komatsu M and Mizushima N (2017) Autophagy-monitoring and autophagy-deficient mice. Autophagy 13:1619-1628. doi: 10.1080/15548627.2017.1343770

29. Christensen JL and Weissman IL (2001) Flk-2 is a marker in hematopoietic stem cell differentiation: a simple method to isolate long-term stem cells. Proc Natl Acad Sci U S A 98:14541-6. doi: 10.1073/pnas.261562798

30. Kiel MJ, Yilmaz OH, Iwashita T, Yilmaz OH, Terhorst C and Morrison SJ (2005) SLAM family receptors distinguish hematopoietic stem and progenitor cells and reveal endothelial niches for stem cells. Cell 121:1109-21. doi: 10.1016/j.cell.2005.05.026

31. Pietras EM, Reynaud D, Kang YA, Carlin D, Calero-Nieto FJ, Leavitt AD, Stuart JM, Gottgens B and Passegue E (2015) Functionally Distinct Subsets of Lineage-Biased Multipotent Progenitors Control Blood Production in Normal and Regenerative Conditions. Cell Stem Cell 17:35-46. doi: 10.1016/j.stem.2015.05.003

32. Bowie MB, McKnight KD, Kent DG, McCaffrey L, Hoodless PA and Eaves CJ (2006) Hematopoietic stem cells proliferate until after birth and show a reversible phase-specific engraftment defect. J Clin Invest 116:2808-16. doi: 10.1172/JCI28310

33. Wilson A, Laurenti E, Oser G, van der Wath RC, Blanco-Bose W, Jaworski M, Offner S, Dunant CF, Eshkind L, Bockamp E, Lio P, Macdonald HR and Trumpp A (2008) Hematopoietic stem cells reversibly switch from dormancy to self-renewal during homeostasis and repair. Cell 135:1118-29. doi: 10.1016/j.cell.2008.10.048

34. Liu F, Lee JY, Wei H, Tanabe O, Engel JD, Morrison SJ and Guan JL (2010) FIP200 is required for the cell-autonomous maintenance of fetal hematopoietic stem cells. Blood 116:4806-14. doi: 10.1182/blood-2010-06-288589

35. Mortensen M, Soilleux EJ, Djordjevic G, Tripp R, Lutteropp M, Sadighi-Akha E, Stranks AJ, Glanville J, Knight S, Jacobsen SE, Kranc KR and Simon AK (2011) The autophagy protein Atg7 is essential for hematopoietic stem cell maintenance. J Exp Med 208:455-67. doi: 10.1084/jem.20101145

36. Leveque-El Mouttie L, Vu T, Lineburg KE, Kuns RD, Bagger FO, Teal BE, Lor M,

Boyle GM, Bruedigam C, Mintern JD, Hill GR, MacDonald KP and Lane SW (2015) Autophagy is required for stem cell mobilization by G-CSF. Blood 125:2933-6. doi: 10.1182/blood-2014-03-562660

37. Warr MR, Binnewies M, Flach J, Reynaud D, Garg T, Malhotra R, Debnath J and Passegue E (2013) FOXO3A directs a protective autophagy program in haematopoietic stem cells. Nature 494:323-7. doi: 10.1038/nature11895

38. Ho TT, Warr MR, Adelman ER, Lansinger OM, Flach J, Verovskaya EV, Figueroa ME and Passegue E (2017) Autophagy maintains the metabolism and function of young and old stem cells. Nature 543:205-210. doi: 10.1038/nature21388

39. Redza-Dutordoir M and Averill-Bates DA (2016) Activation of apoptosis signalling pathways by reactive oxygen species. Biochim Biophys Acta 1863:2977-2992. doi: 10.1016/j.bbamcr.2016.09.012

40. Parmar K, Mauch P, Vergilio JA, Sackstein R and Down JD (2007) Distribution of hematopoietic stem cells in the bone marrow according to regional hypoxia. Proc Natl Acad Sci U S A 104:5431-6. doi: 10.1073/pnas.0701152104

41. Spencer JA, Ferraro F, Roussakis E, Klein A, Wu J, Runnels JM, Zaher W, Mortensen LJ, Alt C, Turcotte R, Yusuf R, Cote D, Vinogradov SA, Scadden DT and Lin CP (2014) Direct measurement of local oxygen concentration in the bone marrow of live animals. Nature 508:269-73. doi: 10.1038/nature13034

42. Winkler IG, Barbier V, Wadley R, Zannettino AC, Williams S and Levesque JP (2010) Positioning of bone marrow hematopoietic and stromal cells relative to blood flow in vivo: serially reconstituting hematopoietic stem cells reside in distinct nonperfused niches. Blood 116:375-85. doi: 10.1182/blood-2009-07-233437

43. Suda T, Takubo K and Semenza GL (2011) Metabolic regulation of hematopoietic stem cells in the hypoxic niche. Cell Stem Cell 9:298-310. doi: 10.1016/j.stem.2011.09.010

44. Takubo K, Nagamatsu G, Kobayashi CI, Nakamura-Ishizu A, Kobayashi H, Ikeda E, Goda N, Rahimi Y, Johnson RS, Soga T, Hirao A, Suematsu M and Suda T (2013) Regulation of glycolysis by Pdk functions as a metabolic checkpoint for cell cycle quiescence in hematopoietic stem cells. Cell Stem Cell 12:49-61. doi: 10.1016/j.stem.2012.10.011

45. Sikorska D, Grzymislawska M, Roszak M, Gulbicka P, Korybalska K and Witowski J (2017) Simple obesity and renal function. J Physiol Pharmacol 68:175-180.

46. Nakamura-Ishizu A, Ito K and Suda T (2020) Hematopoietic Stem Cell Metabolism during Development and Aging. Dev Cell 54:239-255. doi: 10.1016/j.devcel.2020.06.029

47. Huang J, Nguyen-McCarty M, Hexner EO, Danet-Desnoyers G and Klein PS (2012) Maintenance of hematopoietic stem cells through regulation of Wnt and mTOR pathways. Nat Med 18:1778-85. doi: 10.1038/nm.2984

48. Fernandes H, Moura J and Carvalho E (2021) mTOR Signaling as a Regulator of Hematopoietic Stem Cell Fate. Stem Cell Rev Rep 17:1312-1322. doi: 10.1007/s12015-021-10131-z

49. Tamura N, Nishimura T, Sakamaki Y, Koyama-Honda I, Yamamoto H and Mizushima N (2017) Differential requirement for ATG2A domains for localization to autophagic membranes and lipid droplets. FEBS Lett 591:3819-3830. doi: 10.1002/1873-3468.12901

50. Bailey AP, Koster G, Guillermier C, Hirst EM, MacRae JI, Lechene CP, Postle AD and Gould AP (2015) Antioxidant Role for Lipid Droplets in a Stem Cell Niche of Drosophila. Cell 163:340-53. doi: 10.1016/j.cell.2015.09.020

51. Olzmann JA and Carvalho P (2019) Dynamics and functions of lipid droplets. Nat Rev Mol Cell Biol 20:137-155. doi: 10.1038/s41580-018-0085-z

52. Welte MA and Gould AP (2017) Lipid droplet functions beyond energy storage. Biochim Biophys Acta Mol Cell Biol Lipids 1862:1260-1272. doi: 10.1016/j.bbalip.2017.07.006

53. Manesia JK, Xu Z, Broekaert D, Boon R, van Vliet A, Eelen G, Vanwelden T, Stegen S, Van Gastel N, Pascual-Montano A, Fendt SM, Carmeliet G, Carmeliet P, Khurana S and Verfaillie CM (2015) Highly proliferative primitive fetal liver hematopoietic stem cells are fueled by oxidative metabolic pathways. Stem Cell Res 15:715-721. doi: 10.1016/j.scr.2015.11.001

54. Roy IM, Biswas A, Verfaillie C and Khurana S (2018) Energy Producing Metabolic Pathways in Functional Regulation of the Hematopoietic Stem Cells. IUBMB Life 70:612-624. doi: 10.1002/iub.1870

55. Gurumurthy CB, Sato M, Nakamura A, Inui M, Kawano N, Islam MA, Ogiwara S, Takabayashi S, Matsuyama M, Nakagawa S, Miura H and Ohtsuka M (2019) Creation of CRISPR-based germline-genome-engineered mice without ex vivo handling of zygotes by i-GONAD. Nat Protoc 14:2452-2482. doi: 10.1038/s41596-019-0187-x

56. Dobin A, Davis CA, Schlesinger F, Drenkow J, Zaleski C, Jha S, Batut P, Chaisson M and Gingeras TR (2013) STAR: ultrafast universal RNA-seq aligner. Bioinformatics 29:15-21. doi: 10.1093/bioinformatics/bts635

57. Li B and Dewey CN (2011) RSEM: accurate transcript quantification from RNA-Seq data with or without a reference genome. BMC Bioinformatics 12:323. doi: 10.1186/1471-2105-12-323

58. Bray NL, Pimentel H, Melsted P and Pachter L (2016) Near-optimal probabilistic RNA-seq quantification. Nat Biotechnol 34:525-7. doi: 10.1038/nbt.3519

59. Love MI, Huber W and Anders S (2014) Moderated estimation of fold change and dispersion for RNA-seq data with DESeq2. Genome Biol 15:550. doi: 10.1186/s13059-014-0550-8

60. Hochberg Y (1988) A sharper Bonferroni procedure for multiple tests of significance Biometrika 75:3.

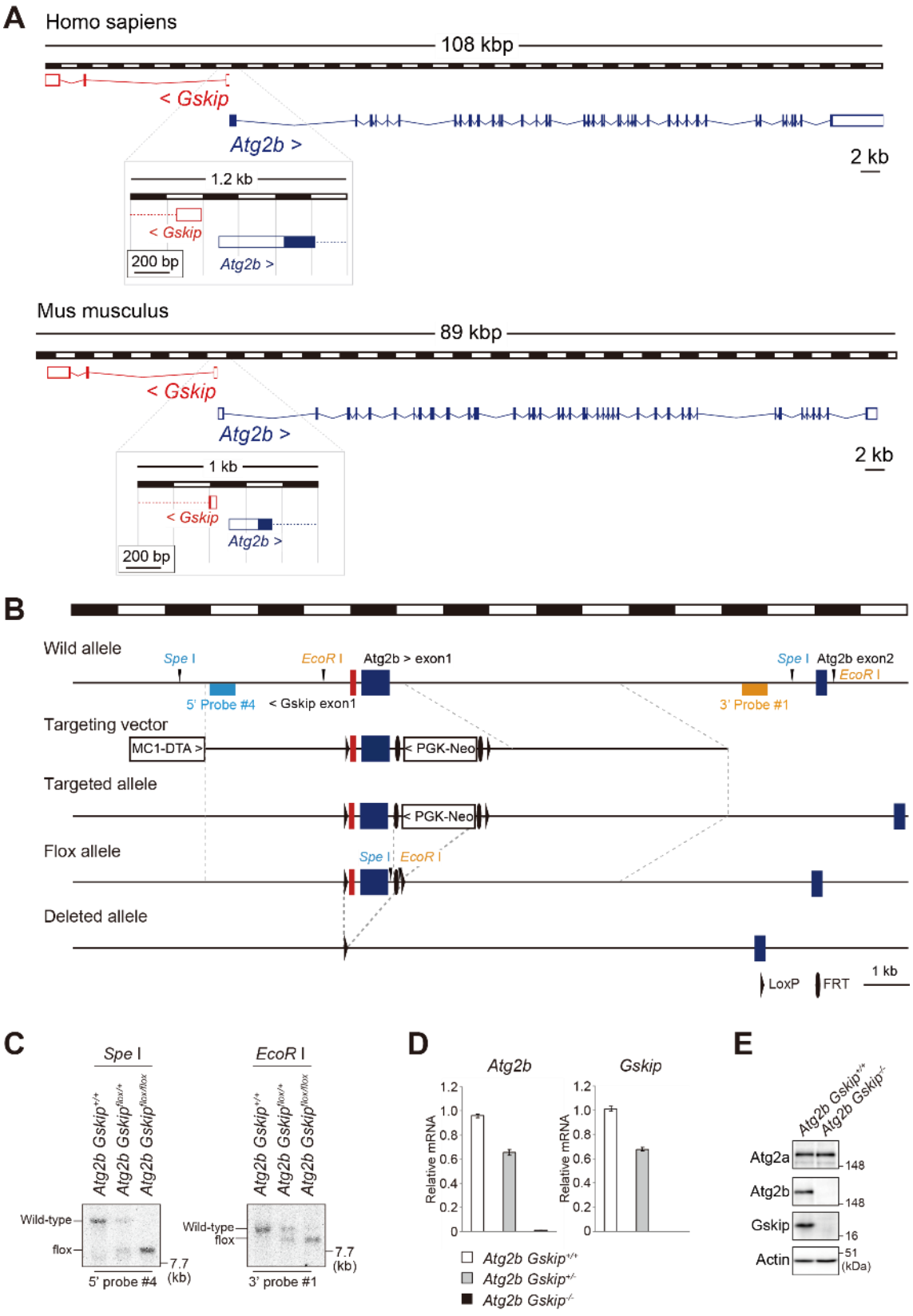

Figure 1

Figure 1 Generation of *Atg2b Gskip*$^{-/-}$ mice. (**A**) Genomic structures of human and mouse

ATG2B and *GSKIP*. (**B**) Schematic representation of the targeting vector and the targeted allele of the *Atg2b* and *Gskip* genes. *Spe*I, *Spe*I sites; *EcoR*I, *EcoR*I site; Neo, neomycin resistance gene cassette; DTA, diphtheria toxin gene. (**C**) Southern blot of genomic DNAs extracted from mouse tails. Wild-type and flox alleles are detected as 16.5- and 9-kb bands or 10.5- and 8.9-kb bands, respectively. Expression of *Atg2b* and *Gskip* transcripts and proteins in double-deficient mouse embryonic fibroblasts. (**D**) Real-time PCR analysis. Total RNA was prepared from indicated genotype MEFs. Values were normalized against the amount of mRNA in the wild-type MEFs. (**E**) Immunoblot analysis. Lysates prepared from indicated genotype MEFs were subjected to SDS-PAGE followed by immunoblot analysis with the indicated antibodies. Data shown are representative of three separate experiments.

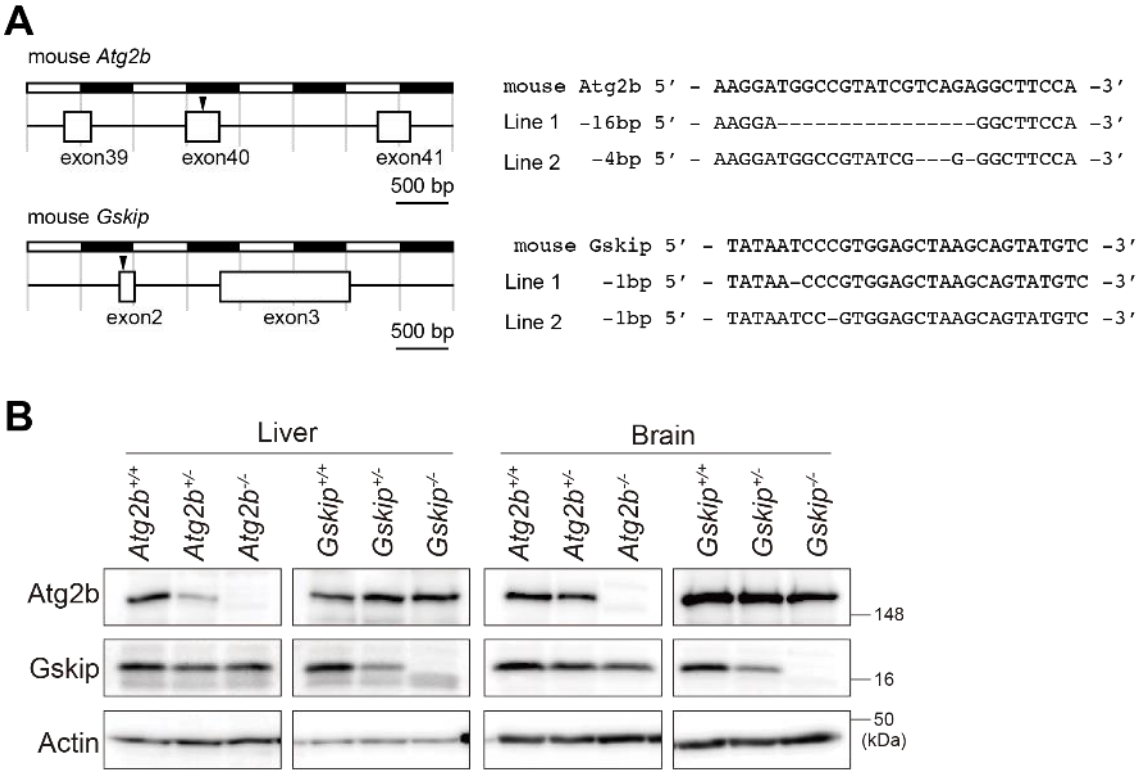

Figure 2

690

Figure 2 Generation of *Atg2b* and *Gskip* single knockout mice. (**A**) Positions of gRNA-targeted sequences in mouse *Atg2b* and *Gskip*, and sequences of the mutant alleles from *Atg2b*- and *Gskip*-deficient mice. Each mutation is highlighted. (**B**) Immunoblot analysis. Homogenates of the livers and brains of mice with the indicated genotypes were subjected to SDS-PAGE
695 followed by immunoblot analysis with anti-Atg2b, Gskip, and Actin antibodies.

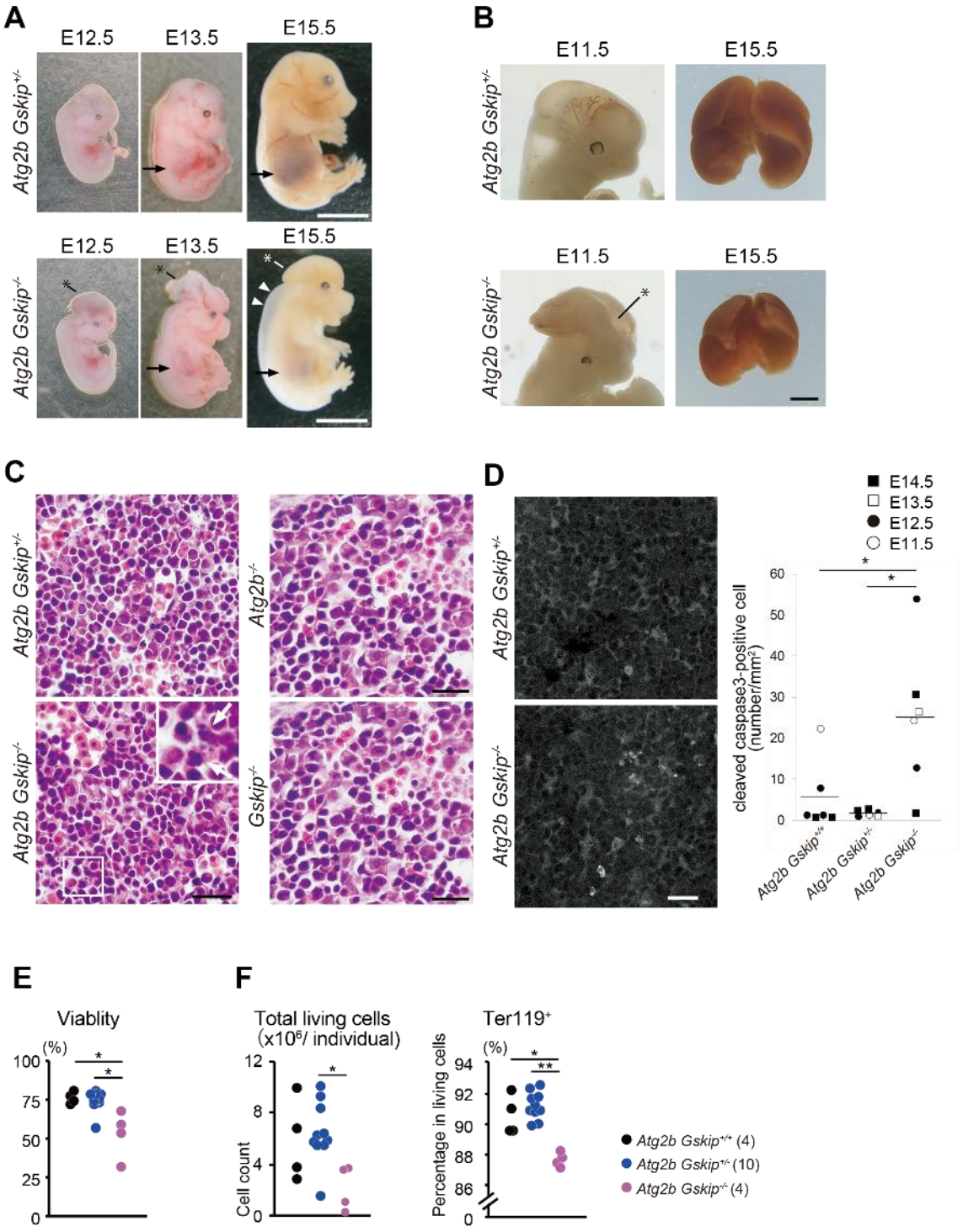

Figure 3

Figure 3 Developmental defects of *Atg2b Gskip*$^{-/-}$ mice. (**A** and **B**) Representative photographs of *Atg2b Gskip* double knockout embryos and heterozygous embryos at E12.5, E13.5, and
700 E15.5. *Atg2b Gskip*$^{-/-}$ embryos exhibited exencephaly (asterisks in A and B) and edema (white

arrowheads). An anemic phenotype can be seen throughout the body, appearing at E15.5, and in liver areas (arrowheads). A representative liver of an *Atg2b Gskip*$^{-/-}$ embryo is smaller than the liver of a heterozygous embryo (B). Bars: 5 mm (A) and 1 mm (B). (**C**) HE staining in fetal liver sections of indicated genotypes. Bars: 20 μm. (**D**) Immunohistofluorescence with anti-cleaved caspase-3 antibody in fetal liver sections from *Atg2b Gskip*$^{+/-}$ and *Atg2b Gskip*$^{-/-}$ at E13.5. Nuclear fragmentation is detected in the mutant liver (arrows in inset). Bars: 20 μm. Cleaved caspase-3–positive cells (per mm^2) were counted in the indicated genotype liver sections at E11.5-14.5 and are plotted in the graph. Horizontal bars indicate mean values. (**E**) Percentage (left) and total (right) living cells in fetal liver of mice at E13.5. (**F**) The percentage of Ter119$^+$ erythroid cells in living cells. Numbers of embryos used for each analysis are shown in parentheses. *: $P < 0.05$ as determined by Mann-Whitney *U* test. ns: not significant.

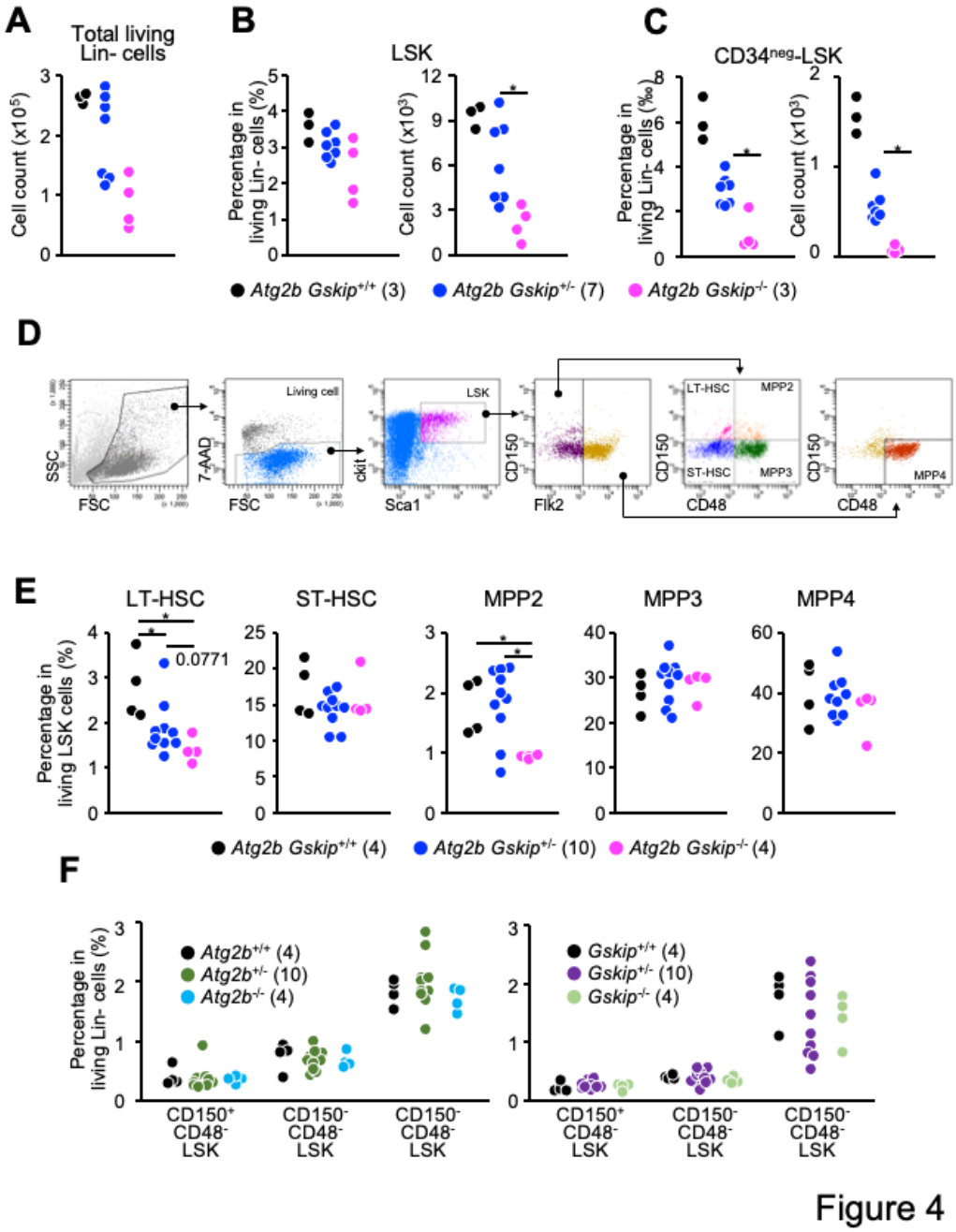

Figure 4

Figure 4 Impairment of hematopoiesis in E13.5 *Atg2b Gskip*$^{-/-}$ embryos. (**A**) The absolute number of living Lin(-) cells per liver. (**B**) The percentage of LSK cells in living Lin(-) cells (left) and the absolute number of LSK cells per liver (right) (**C**) The percentage of CD34^{neg}-

LSK cells in living Lin(-) cells (left) and the absolute number of $CD34^{neg}$-LSK cells per liver (right). (**D**) Representative gating strategy used to identify LT-HSC, ST-HSC, MPP2, MPP3, and MPP4. (**E**) The percentages of LT-HSCs, ST-HSCs, MPP2, MPP3, and MPP4 cells in the
720 LSK fraction. (F) The percentages of $CD150^{+}CD48^{-}$LSK, $CD150^{-}CD48^{-}$LSK, and $CD150^{+}CD48^{+}$LSK cells in living Lin(-) cells in E13.5 *Atg2b*$^{-/-}$ (left) and *Gskip*$^{-/-}$ embryos (right). Numbers of embryos used for each analysis are shown in parentheses. *: $P < 0.05$ as determined by Mann-Whitney *U* test.

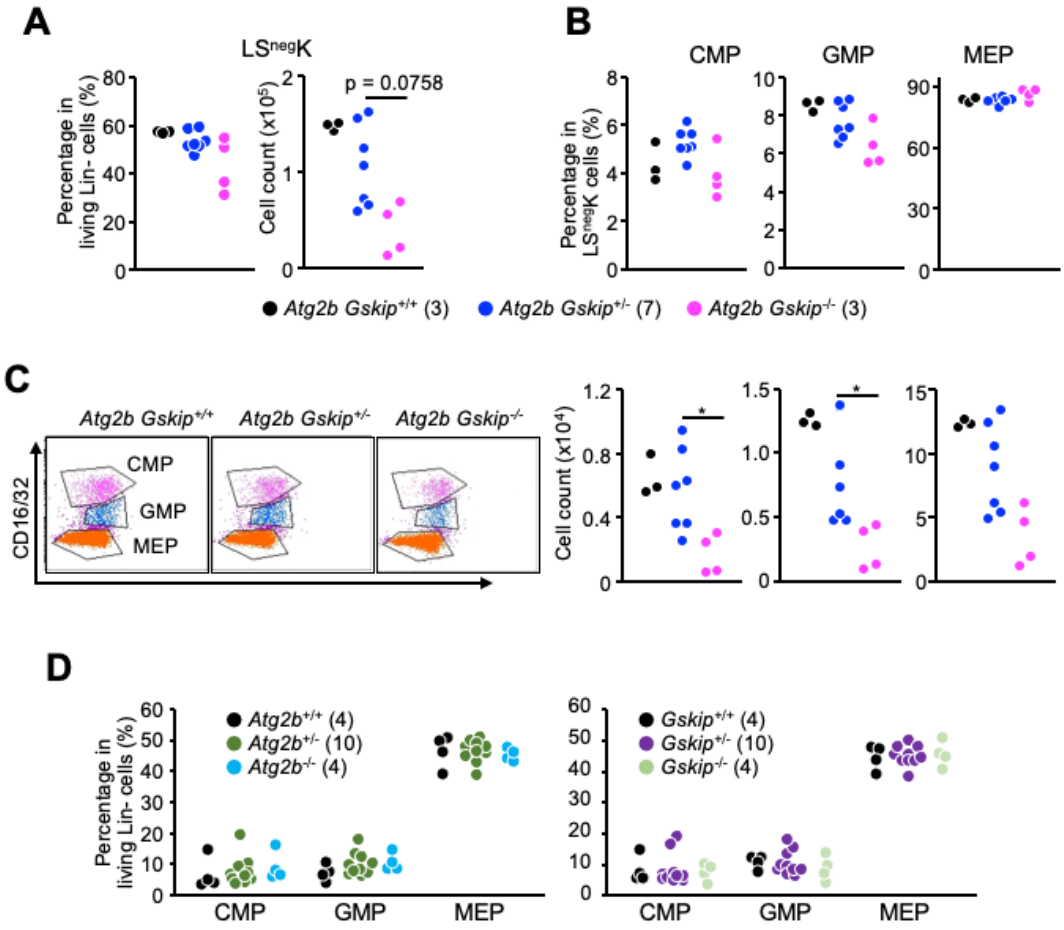

Figure 5

725

Figure 5 Flow cytometric analysis of CMPs, GMPs, and MEPs in embryos. (**A**) The percentage of LS^{neg} cells in living Lin(-) cells (left) and the absolute number of LS^{neg} cells per liver (right). (**B**) The percentages of CMPs, GMPs, and MEPs in $LS^{neg}K$ cells (upper) and the absolute

numbers of CMP, GMP, and MEP cells per liver (lower). (**C**) Representative dot plots of LS^{neg} cells showing CD16/32 and CD34 expression. CMPs, GMPs, and MEPs are defined as indicated. (**D**) The percentages of CMPs, GMPs, and MEPs cells in living Lin(-) cells in E13.5 *Atg2b*$^{-/-}$ (left) and *Gskip*$^{-/-}$ embryos (right). Numbers of embryos used for each analysis are shown in parentheses. *: $P < 0.05$ as determined by Mann-Whitney *U* test.

A

		Atg2b Gskip $^{+/+}$	*Atg2b Gskip* $^{+/-}$
WBC	(x10^2/μL)	138 ± 3	128 ±17
RBC	(x10^4/μL)	940 ± 8	932 ± 21
HGB	(g/dL)	13.5 ± 0.0	13.1 ± 0.6
HCT	(%)	42.1 ± 0.3	41.7 ±1.0
MCV	(fL)	44.8 ± 0.1	44.8 ± 0.3
MCH	(pg)	14.4 ± 0.1	14.1 ± 0.4
MCHC	(g/dL)	32.1 ± 0.2	31.5 ± 1.1
PLT	(x10^4/μL)	102 ± 2	117 ± 11

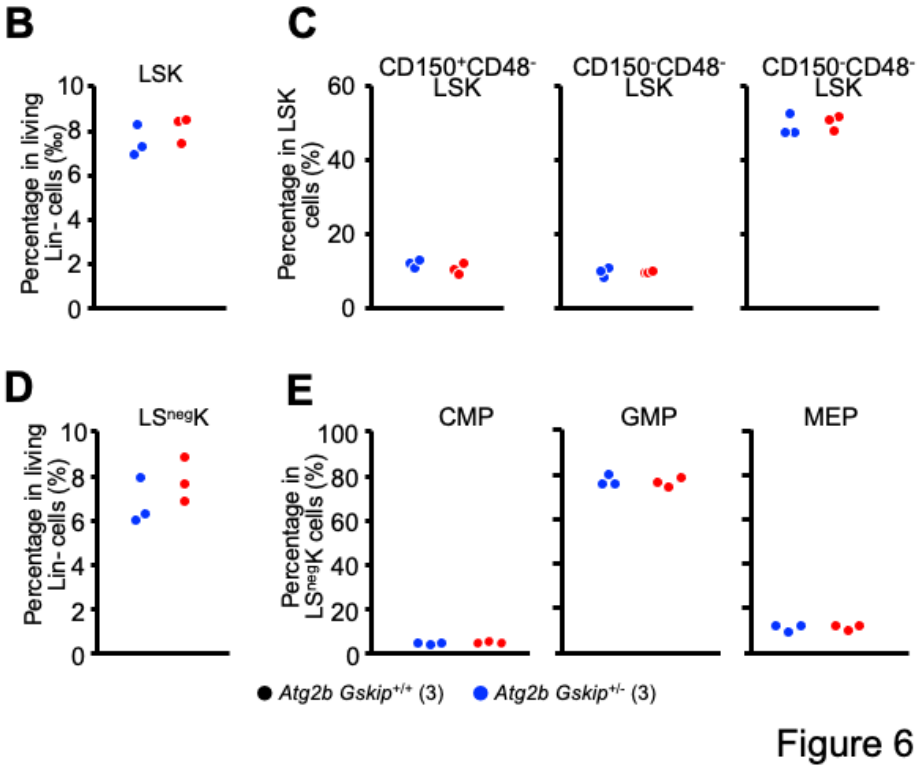

Figure 6

735

Figure 6 Normal hematopoiesis in heterozygous *Atg2b Gskip*$^{+/-}$ adult mice. (**A**) Hematopoietic indices of three *Atg2b Gskip*$^{+/+}$ and three *Atg2b Gskip*$^{+/-}$ mice at 10 weeks old. Mice were bled from the retro-orbital plexus under anesthesia. (**B-E**) Summary of flow cytometry analyses of

three *Atg2b Gskip*$^{+/+}$ and three *Atg2b Gskip*$^{+/-}$ mice at 10 weeks old. The percentage of CD34^{neg}-LSK cells in Lin(-) cells (B), the percentages of LT-HSCs, ST-HSCs, and MPPs in CD34^{neg} LSK cells (C), the percentage of LS^{neg} cells cells in Lin(-) cells (D), and the percentages of CMPs, GMPs, and MEPs in LS^{neg} cells (E) are shown. Numbers of embryos used for each analysis are shown in parentheses.

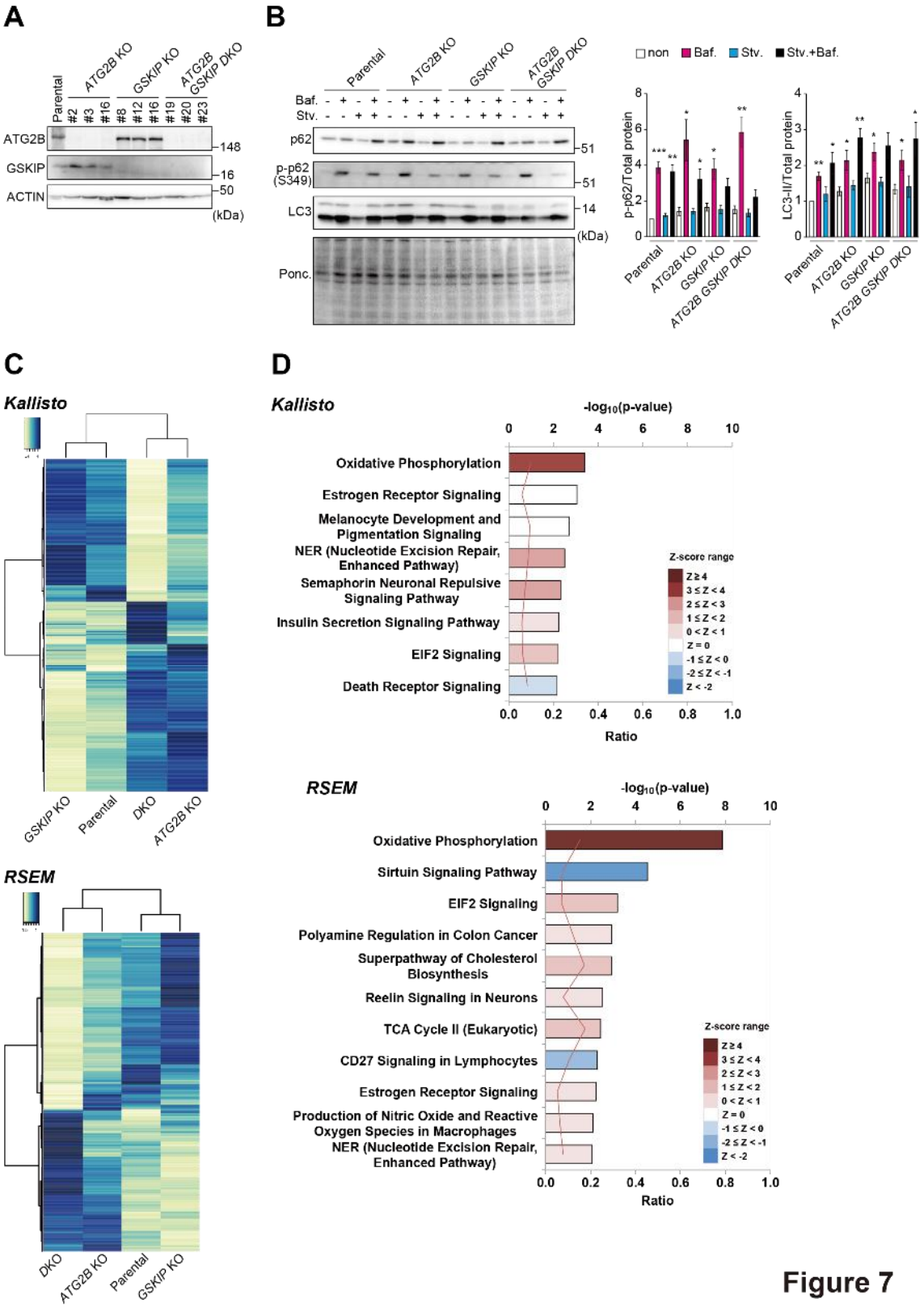

Figure 7

745

Figure 7 Dissection of autophagic activity and gene expression in *ATG2B GSKIP*-deficient K562 cells. (**A** and **B**) Immunoblot analysis. Parental, *ATG2B*-, *GSKIP*-, and *ATG2B GSKIP*-deficient K562 cells were lysed, and then cell lysates were subjected to SDS-PAGE followed by immunoblotting with the indicated antibodies (A). Parental, *ATG2B*-, *GSKIP*-, and *ATG2B*

GSKIP-deficient K562 cells were cultured in nutrient-rich (-) or -deprived (stv.) conditions in the presence or absence of bafilomycin A1 (Baf. A_1). The cell lysates were subjected to SDS-PAGE followed by immunoblot analysis with the indicated antibodies and Ponceau staining (B). Graphs show the levels of LC3-II and S349-phosphorylated p62 per total protein estimated by Ponceau staining. Data shown are representative of four separate experiments. (**C**) Gene clustering. RNA-seq analysis was performed using wild-type (n = 3), *ATG2B* single knockout (n = 3), *GSKIP* single knockout (n = 3), and *ATG2B GSKIP* double knockout K562 cells (n = 3). Hierarchical clustering was performed on differentially expressed genes and is presented as a heatmap. Right and left heatmaps were created using Kallisto and RSEM, respectively. (**D**) Ingenuity Pathway Analysis of the RNA-seq data was used to predict signaling pathway activity. The pathways for which the p-value ≤ 0.01 and the z-score could be calculated are shown. The upper axis shows $-\log_{10}$(P-value), and the lower axis shows the ratio between the number of differentially expressed genes and the number of genes in each pathway. The z-score, which predicts activation (positive values) or inhibition (negative values) of canonical pathways, is shown by the color scale. An absolute z-score ≥ 2 is considered significant.

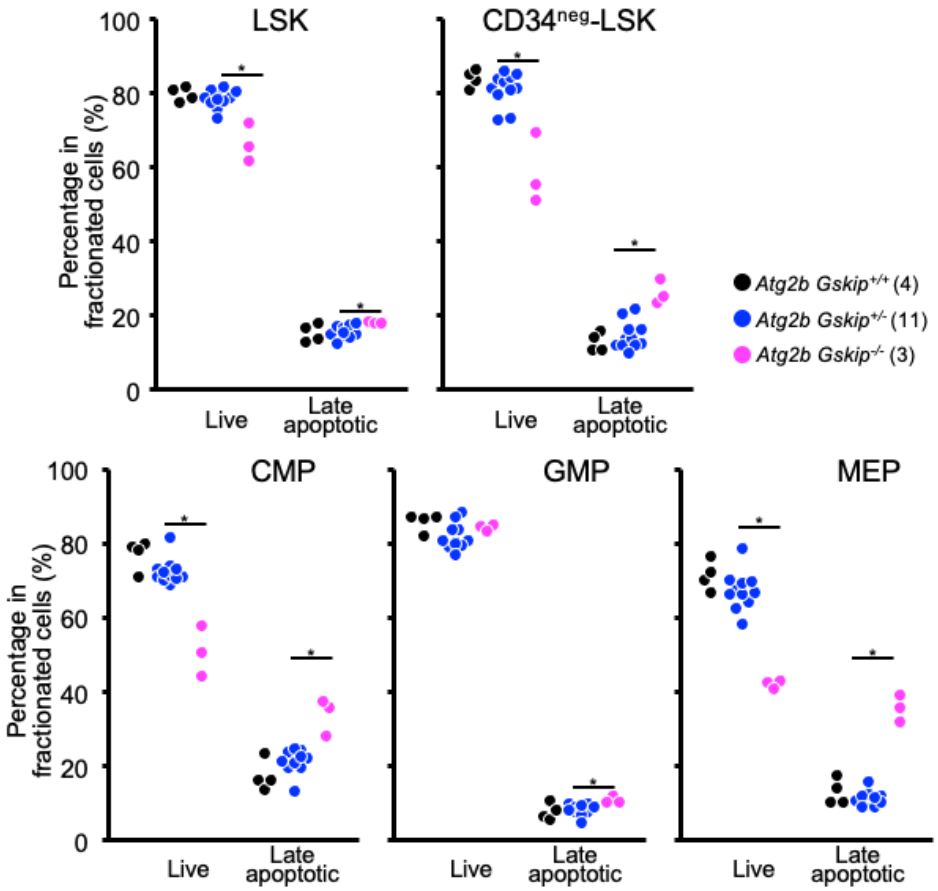

Figure 8

Figure 8 The frequencies of living and late apoptotic cells. (**A-E**) The frequencies of living and late apoptotic cells gated in LSK (A), CD34^{neg}-LSK (B), CMP (C), GMP (D), and MEP fractions (E) are presented. Living and late apoptotic cells were defined as AnnexinV(-)7-

AAD(-) and AnnexinV(+)7-AAD(+), respectively. Four *Atg2b Gskip*$^{+/+}$, 11 *Atg2b Gskip*$^{+/-}$, and three *Atg2b Gskip*$^{-/-}$ embryos were used. Numbers of embryos used for each analysis are shown in parenthesis. *: $P < 0.05$ as determined by Mann-Whitney *U* test.

Table 1. Genotype analyses of *Atg2b Gskip*$^{+/-}$, *Atg2b*$^{+/-}$, *Gskip*$^{+/-}$, and *Atg2a*$^{+/-}$ intercross progeny.

DNA source	Genotype		
	Atg2b Gskip$^{+/+}$	*Atg2b Gskip*$^{+/-}$	*Atg2b Gskip*$^{-/-}$
Amnion (E11.5)	1	10	4
Amnion (E12.5)	5	8	4
Amnion (E13.5)	8	19	8
Amnion (E14.5)	7	13	6
Amnion (E15.5)	1	7	6
Amnion (E16.5)	5	8	1
Tail (P0)	25	39	0

DNA source	Genotype		
	Atg2b$^{+/+}$	*Atg2b*$^{+/-}$	*Atg2b*$^{-/-}$
Tail (4 weeks old)	26	44	23

DNA source	Genotype		
	Gskip$^{+/+}$	*Gskip*$^{+/-}$	*Gskip*$^{-/-}$
Tail (4 weeks old)	20	29	15